Monovacancy Properties of FCC and HCP Structures From Automated Atomistic Simulation Based on OpenKIM

Junhao Li* and James P. Sethna†
Department of Physics and Laboratory of Atomic and Solid State Physics
Cornell University, Ithaca, New York 14853, USA
(Dated: April 11, 2016)

The quality of interatomic models is crucial to atomistic simulations. In this study, we assess the interatomic models in terms of their ability to describe vacancy-related interactions. Based on the OpenKIM framework, we perform automated atomistic calculations of monovacancy properties, including the formation energy, the migration energy, and the relaxation volume, for all the interatomic models currently available in the OpenKIM repository, and compare the calculation results with reference data from density functional (DFT) calculations and experiments to identify the most promising interatomic models for defect-related simulations. We also explore how the monovacancy properties relate to each other, and to other elemental properties.

I. INTRODUCTION

A longtime goal of scientists' is to be able to calculate the properties of materials from their structures accurately and efficiently. There are several approaches to this problem, including density functional theory (DFT) and atomistic simulation. DFT has developed rapidly in the recent few decades and achieved decent accuracy for many small-scale systems. However, in many cases, the size, the complexity, or the timescale we want to simulate, demands a much more efficient method. And atomistic simulation with good interatomic potentials is one of the methods that can fulfill this demand.

Several different types of interatomic models have been developed over the past few decades, from pairwise models like Lennard-Jones, to those based on cluster functionals, such as embedded-atom method (EAM) [1, 2]. One problem that has hindered the development of atomistic simulation is that the models developed by various researchers are usually presented in different formats, making them difficult to be reused. The OpenKIM project [3, 4] solves this problem by providing a unified framework for model developers to submit, and for model users to perform atomistic simulations with these models [5]. It also hosts a repository of reference data from other sources, such as DFT and experiments, to assess the quality of these models.

In this study, we focus on the simulation of vacancies. Finding interatomic models that can accurately describe vacancy effects is extremely beneficial for furthering our understanding and application of materials. Vacancies are the simplest and the most common defects. They affect dislocation climbing and creeping [6], mediate the diffusion of substitutional defects [7], and are the dominant flow mechanism under external fields, such as gravity [8]. Also, some scientists are proposing using ^{28}Si for a new kilogram definition [9], and how to obtain the vacancy concentration accurately will be a crucial part of this work.

Here we use OpenKIM to calculate, automatically, the most important vacancy-related properties, including the vacancy formation energy (VFE) and the vacancy migration energy (VME), and compare the results with the reference data from DFT calculations and experiments. In doing so, we can help researchers who care about vacancy effects in their atomistic simulation choose models that are more suitable for them.

The vacancy relaxation volume (VRV) is also an important property, determining vacancies' response to internal and external stresses. Therefore, we calculate and report it in this study as well, although we do not have the reference data available for it at this time.

In addition, we also explore how these properties relate to each other, and to other elemental properties, such as the cohesive energy and the bulk modulus.

The paper is organized as follows. In Sec. II we describe the algorithm used for calculating the monovacancy properties. In Sec. III we show the plots of our results, compare them with the reference data, and explore how they relate to each other and to other elemental properties. Sec. V concludes this paper. And Appendix B list the scripts used for obtaining the data from OpenKIM.

II. METHODOLOGY

We calculate the three most important monovacancy-related properties in crystals: the formation energy (VFE), the migration energy (VME), and the relaxation volume (VRV). The definitions for these properties can be found at `https://openkim.org/properties`.

The calculation is based on OpenKIM and the Atomic Simulation Environment (ASE) [10]. We first obtain the lattice constants through energy minimization, and then use this value to build several periodically repeated supercells of different sizes. For each supercell, we use the following algorithm to obtain the desired properties:

* jl2922@cornell.edu
† sethna@lassp.cornell.edu

1. Obtain the potential energy and volume of this supercell, E_0 and V_0.
2. Remove an atom, relax the positions of the other atoms (keep the size of the supercell fixed) and obtain the new potential energy, E_1.
3. Calculate the vacancy formation energy by:
$$VFE = E_1 - E_0 \times \frac{n-1}{n} \tag{1}$$
where n is the number of atoms in the original supercell.
4. Move one atom to the vacant site from the nearest neighbors and use the nudged elastic band (NEB) method to obtain the saddle point energy, E_2.
5. Calculate the vacancy migration energy by:
$$VME = E_2 - E_1 \tag{2}$$
6. Relax the size of the supercell and obtain the relaxation volume.

Finally, we extrapolate these results to get the dilute limit. The extrapolation is based on the elastic theory [11], according to which all the quantities that we are interested in scale approximately as

$$A_0 + \frac{A_3}{n} \tag{3}$$

where n is the number of atoms in a supercell [12], and A_0 and A_3 are the constants to be determined. A_0 is the dilute limit we want.

We can prove this scaling relationship as follows: first of all, $n \propto R^3$, where R is the size of the supercell, so Eq. (3) is equivalent to $A_0 + A_3/R^3$. For simplicity, we ignore anisotropy and nonlinearity, and consider the supercell with a vacancy as a hollow sphere. According to the elastic theory, the displacement vector of a hollow sphere of external and internal radii R_1 and R_2 with a pressure p_1 inside and p_2 outside is $\vec{u} = \left(ar + b/r^2\right)\hat{r}$, where

$$a = \frac{p_1 R_1^3 - p_2 R_2^3}{R_2^3 - R_1^3} \cdot \frac{1-2\sigma}{E} \tag{4}$$

$$b = \frac{R_1^3 R_2^3 (p_1 - p_2)}{R_2^3 - R_1^3} \cdot \frac{1+\sigma}{2E} \tag{5}$$

Here σ is the Poisson's ratio, E is the Young's modulus, $p_2 = 0$, and, for VRV, $r = R_2$. Hence, we can get the r component of $\vec{u}$

$$u_r = \frac{p_1 R_1^3}{R_2^2} \cdot \frac{3\,(1-\sigma)}{2E}\left(1 + \frac{R_1^3}{R_2^3} + O\left(\frac{1}{R_2^6}\right)\right) \tag{6}$$

Therefore, the vacancy relaxation volume

$$\begin{aligned} VRV &= \frac{4}{3}\pi\left(R_2^3 - (R_2 - u_r)^3\right) \\ &= 4\pi C_0\left(1 + \frac{R_1^3 - C_0}{R_2^3} + O\left(\frac{1}{R_2^6}\right)\right) \end{aligned} \tag{7}$$

Here $C_0 = 3p_1 R_1^3(1-\sigma)/2E$ is a constant. Eq. (7) indicates that VRV satisfies Eq. (3).

The strain and the stress of the hollow sphere are

$$u_{rr} = a - 2b/r^3 \tag{8}$$

$$u_{\theta\theta} = u_{\phi\phi} = a + b/r^3 \tag{9}$$

$$\sigma_{rr} = \frac{pR_1^3}{R_2^3 - R_1^3} \cdot \left(1 - \frac{R_2^3}{r^3}\right) \tag{10}$$

$$\sigma_{\theta\theta} = \sigma_{\phi\phi} = \frac{p_1 R_1^3}{R_2^3 - R_1^3} \cdot \left(1 + \frac{R_2^3}{r^3}\right) \tag{11}$$

From these we can obtain the vacancy formation energy

$$\begin{aligned} VFE &= \iiint_V \frac{1}{2}\left(u_{rr}\sigma_{rr} + u_{\theta\theta}\sigma_{\theta\theta} + u_{\phi\phi}\sigma_{\phi\phi}\right) dV \\ &= 4C_1(1+\sigma) + 2C_1C_2 \cdot \frac{R_1^3}{R_2^3} + O\left(\frac{1}{R_2^6}\right) \end{aligned} \tag{12}$$

where $C_1 = p_1^2\pi R_1^3/(3E)$ and $C_2 = 5 - 4\sigma + (6\sigma - 3)\log(R_1/R_2)$. This proves that VFE scales approximately as Eq. (3).

Note that, for efficiency, our calculation of VFE is performed with a fixed-size supercell, not a stress-free one. This will not affect the results, because the difference between the results from the two different boundary conditions is

$$\Delta E = \int p dV = \int B\frac{V - V_0}{V_0} dV \propto \frac{(V - V_0)^2}{V_0} \tag{13}$$

where the numerator is $VRV^2 = 16\pi C_0^2 + O(R_2^{-3})$, and the denominator is proportional to R_2^3. This means ΔE also scales as $1/R_2^3$.

VME is the energy difference between two configurations: a crystal with a monovacancy, and a crystal with two monovacancies adjacent to each other and an extra atom somewhere between the two vacant sites. The energy of the first configuration has just been proved to scale as Eq. (3). The second configuration can be considered as a superposition of three states: two states correspond to the initial and final states of the migration, and the third one corresponds to the saddle point but with the two vacant sites filled up. The proof of VFE can be applied directly to each of these states and give similar R_2 dependencies. Therefore, VME also satisfies Eq. (3).

Fig. 1 is a plot of VFE versus $1/n$, calculated with the EAM model of aluminum from Mishin and Farkas [13]. In this case, $A_0 = 0.67515(1)$ eV and $A_3 = -0.3644(27)$ eV, which implies that the monovacancy formation energy is 0.67515(1) eV. The linear relationship shown in this figure and the adjusted R-square of 0.99978 in the fitting validate our extrapolation.

The code that implements the whole algorithm is available in the OpenKIM repository [4], id: 554849987965.

FIG. 1. Monovacancy formation energy (VFE) versus the inverse of the number of atoms (n) in a supercell, calculated with the embedded atom model (EAM) of aluminum from Mishin and Farkas [13]. As we can see from this plot, there is a strong linear correlation between VFE and $1/n$. The adjusted R-square of the linear fitting is 0.99978. The intercept of the fitted line corresponds to VFE of the dilute limit 0.67515(1) eV.

III. RESULTS AND DISCUSSION

A. Calculated Results Versus Reference Data

All the results calculated in this work are available in the OpenKIM repository [4]. In Appendix A, we list the scripts that can automatically retrieve these results through OpenKIM Query, the data querying API provided by OpenKIM.

Comparison of our results and the reference data from DFT calculations and experiments can be found in Fig. 2, where Fig. 2(a) and 2(b) are the results for fcc structures, and Fig. 2(c) and 2(d) are the results for hcp structures. The red dots and the blue dots in these figures represent the reference data from DFT calculations and experiments, respectively. The black symbols represent the results from atomistic simulations. The type of the interatomic model is indicated by the shape of the symbol: the circles represent the embedded-atom method (EAM), the triangles represent the pairwise models, and the cross signs represent all the other types of models, such as the three-body models.

We can see from these figures that the EAM models, in general, produce similar VFE and VME as DFT calculations and experiments. While most pairwise models tend to produce larger values for VFE, especially for elements with Mendeleev numbers ranging from 25 to 45, which correspond to the transition metals and the post-transition metals.

One explanation for the pairwise models to get larger VFE could be that pairwise models assume the strength of the bonds only depend on the distance between the two atoms. They ignore the fact that the change in the number of bonds can also affect the strength of the bonds, and thus the energy.

To see this in detail, we exam the unrelaxed vacancy formation energy, *UnrelaxedVFE*, which the vacancy formation energy without position relaxation. It consists of three parts, which can be expressed by

$$UnrelaxedVFE = N \cdot E_{bond} + \sum \Delta E_{bond} - E_{coh} \quad (14)$$

where N is the number of bonds surrounding each atom. The first term corresponds to the breaking of the bonds between the vacant site and its nearest neighbors. We ignore the contribution from breaking the bonds between the vacant site and its second nearest neighbors because it is much smaller than the first term. The second term corresponds to the energy change in the remaining bonds. And the third term is the cohesive energy, corresponding to the $n-1$ in Eq. (1), which also equals to $N \cdot E_{bond}/2$, as the energy of each bond is shared between the two atoms it connects. For all the pairwise models, we shall have $UnrelaxedVFE \approx E_{coh}$, as $\sum \Delta E_{bond}$ is zero; while for all the models that do take changes in the surrounding environment into consideration besides the distance between two atoms, we shall have *UnrelaxedVFE* significantly different from E_{coh}. In Table I we show our verification: the pairwise models do get similar values for *UnrelaxedVFE* and E_{coh}, while other types of models get significantly different values.

===(Draft of draft below this line)===

In Table I, we show an example of fcc copper: as we move the atom next to the vacant slight away from the original position, the change in the cohesive energy according to the EAM potential is about 40% smaller than the value according to the pairwise potential. This implies that as we create vacancy and remove bonds, the strength of the remaining bonds may decrease. We propose that the vacancy formation energy can be expressed as

$$VFE = E_{cohesive} + \Delta E_{bonds,all} + \Delta E_{relaxation} \quad (15)$$

Where $\Delta E_{bonds,all}$ is the change in the bond energy and the $\Delta E_{relaxation}$ is the change in energy due to position relaxation. When we remove an atom, all the bonds associated with that atom are also removed, which means the energy change is $n \times E_{bond}$, where n is the number of bonds surround each atom and E_{bond} is the energy of a single bond. Since each bond is associated with two atoms, thus the cohesive energy, $E_{cohesive}$, of an atom shall be the energy of half of the bonds associated with

TABLE I. Relationship between the cohesive energy, E_{coh}, and the unrelaxed vacancy formation energy, *UnrelaxedVFE*, calculated for fcc structures with different types of models. We can see that the pairwise models do get similar values for these two items while other types of models do get significantly different values. All the models can be found in the OpenKIM repository by the ID numbers shown in the footnotes.

Model	E_{coh}/eV	*UnrelaxedVFE*/eV
Pairwise Al[a]	2.7004	2.7004
Pairwise Cu[a]	3.2741	3.2741
EAM Al[b]	3.3599	0.7691
EAM Cu[c]	3.5193	1.2196
EMT Al[d]	3.2788	0.9806
EMT Cu[d]	3.2213	1.2788

[a] (ID: 411898953661_001(Al) and 673777079812_001(Cu)) Morse pair potential with parameters from Girifalco and Weizer, 1959.
[b] (ID: 651801486679_001) EAM Al potential with parameters from Mishin et al., 1999.
[c] (ID: 179025990738_001) EAM Cu potential with parameters from Ackland et al., 1987.
[d] (ID: 118428466217_002) EMT implementation in ASAP by Jacobsen et al.

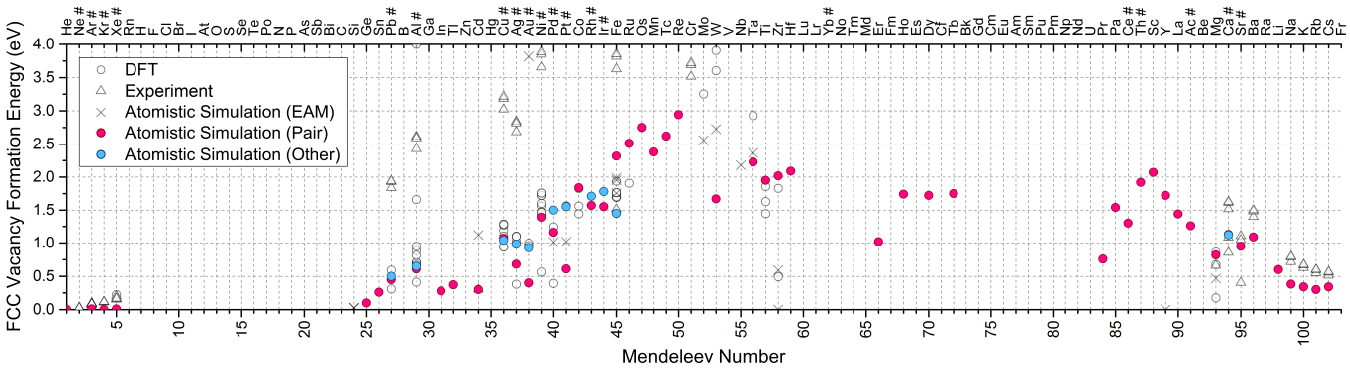

(a)

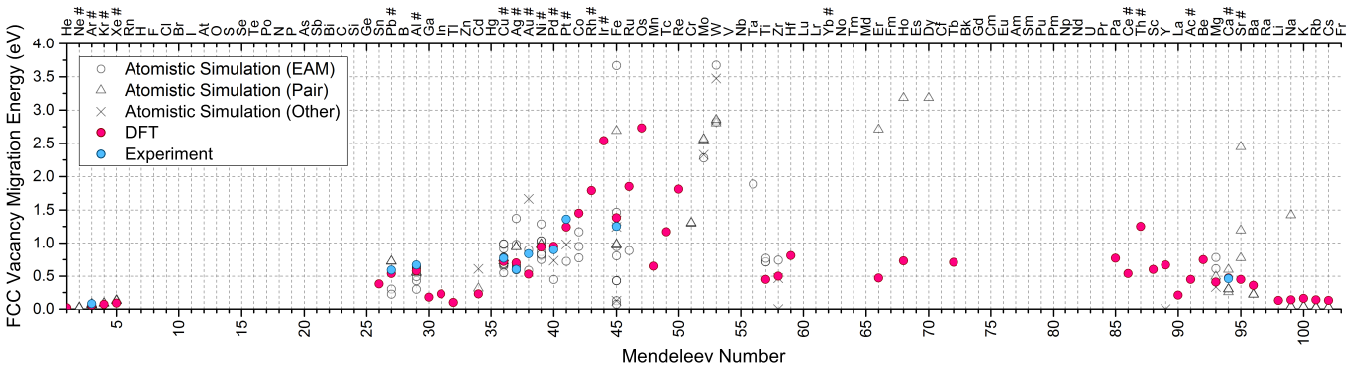

(b)

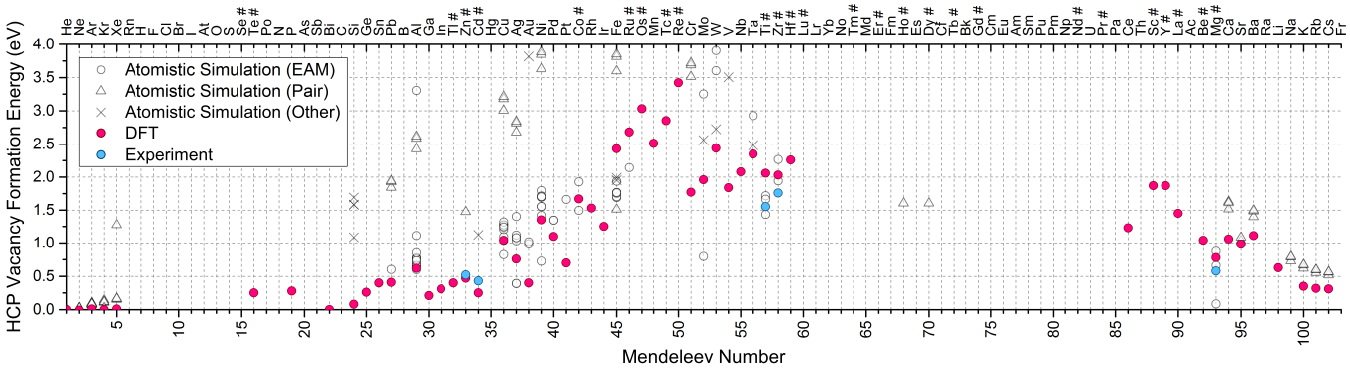

(c)

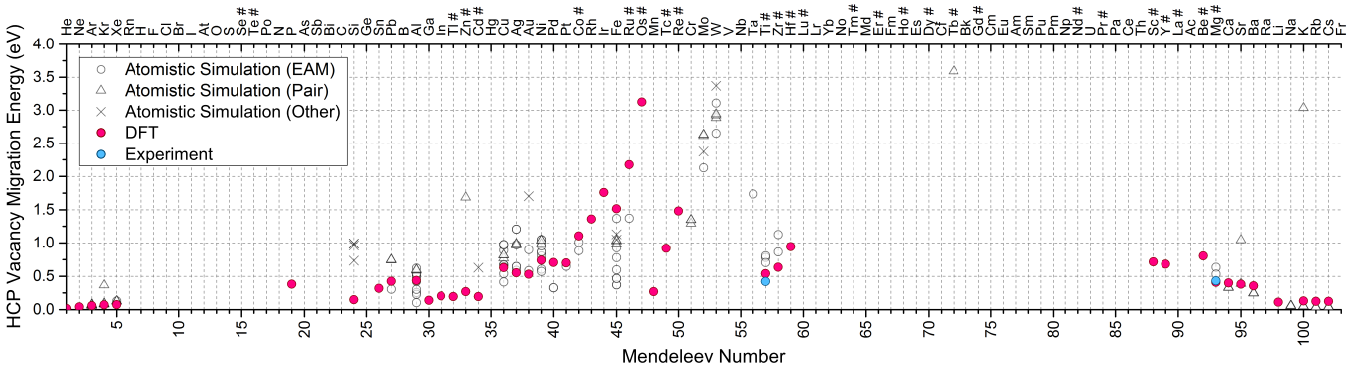

(d)

FIG. 2. Comparison of the results from our atomistic simulations and the reference data, where Fig. (a) and (b) are the results for fcc structures, and Fig. (c) and (d) are the results for hcp structures. The '#' sign next to the symbol of each element indicates whether the structure presented by the figure is the element's natural state.

TABLE II. Change in the cohesive energy of fcc copper as we move the atom next to the vacant slight slightly along the x direction away from the original position.

Displacement (Å)	EAM[a] (eV)	Pairwise[b] (eV)
0.01	0.000	0.000
0.02	0.001	0.002
0.04	0.005	0.009
0.08	0.021	0.037
0.16	0.092	0.148
0.32	0.407	0.596
0.64	1.649	2.440
1.28	5.383	9.306
2.56	13.37	41.91
5.12	10.31	22.04

[a] EAM_Dynamo_Ackland_Tichy_Cu.
[b] Pair_Morse_Shifted_GirifalcoWeizer_LowCutoff_Cu.

the atom, that is $n \times E_{bond}/2$. Compare with Eq. (1), we can get the first $E_{cohesive}$ term in Eq. 15. For pairwise potentials, $\Delta E_{bonds,all}$ is zero and $\Delta E_{relaxation}$ is usually much smaller than $E_{cohesive}$, so the vacancy formation energy according to them will be very close to the cohesive energy. This can be verified with our data. For example, with a pairwise potential for fcc copper, we will get the cohesive energy is 3.27 eV and the vacancy formation energy is 3.02 eV. We have also verified that without relaxation (no $\Delta E_{relaxation}$), the unrelaxed vacancy formation energy is also 3.27 eV, same as $E_{cohesive}$.

For pairwise potentials, the bond energy per atom increase linearly with the number of bonds. However, experiments show there is a quadratic relationship between them. This implies that when we remove a bond, the strength of the remaining bonds will be weakened. Therefore, the change in energy during position relaxation will be smaller than if the bond strength remains the same. And this change in energy is exactly the main component of the vacancy formation energy.

Other types of potentials sometimes also produce accurate results but are only available to a few elements. This suggests that right now in general EAM is the most promising method for describing vacancy effects. We believe there are several reasons why EAM outperforms other methods:

1. EAM incorporates the multibody effects, which is crucial for describing the interaction between atoms.

2. The training data for the EAM potentials usually includes both experimental data and DFT calculation results.

3. For the EAM potentials, most of the information contained in the training data is kept into the potential models, while for other fixed-form potentials, lots of information is lost during the fitting process.

In Table IV, we list the models currently available on OpenKIM that are most consistent with DFT and experiments. They are selected based on the mean absolute percentage error (MAPE), a measure of prediction accuracy of models used in statistics, which in this case is defined as the average relative error to our reference data

$$MAPE = \frac{1}{n} \sum_i \left| \frac{C_i - R_i}{R_i} \right| \tag{16}$$

Here n is the number of reference data available for the items we successfully calculate, C_i is the calculated value, and R_i is the reference value. The value of $MAPE$ for each model in this table is shown in column 4. Note that in our reference data, the mean absolute percentage error between the DFT results and experimental results is 27.87%. Comparing to this, we can see that for most of the elements in this table, there exists a potential that can produce reasonably accurate results. These potentials are all good candidates for atomistic simulation when vacancy effects are significant.

We can also see from these two tables that for nearly all the elements that have EAM potentials, the EAM potentials are selected as the best models in Table IV according to the criteria above. Only in very few cases, other types of potentials perform better than the EAM potentials. This is consistent with our previous analysis.

B. Relationship to Other Properties

We plot the vacancy property results from our atomistic simulation against cohesive energy and bulk modulus in Fig. 3. Both the cohesive energy and bulk modulus are obtained from the Materials Project [14, 15]. Here we use the same symbol as in Fig. 2: the circles represent embedded-atom method (EAM), the triangles represent pairwise potentials, and the cross signs represent all the other types of potentials, such as three-body potentials.

We can see from these plots that as cohesive energy increases, vacancy formation energy and migration energy also increase. This is consistent with previous results from DFT [16].

IV. CONCLUSION

In this study, we assess the quality of interatomic models currently available in the OpenKIM repository `https://openkim.org/intro-models/`, in terms of their ability to describing vacancy-related properties.

We first develop tests using the OpenKIM API to perform the atomistic calculation of three most important monovacancy properties, the vacancy formation energy, the vacancy migration energy and the relaxation energy, for all the available interatomic models. Then we compare the calculation results with reference data from density functional (DFT) calculations and experiments by

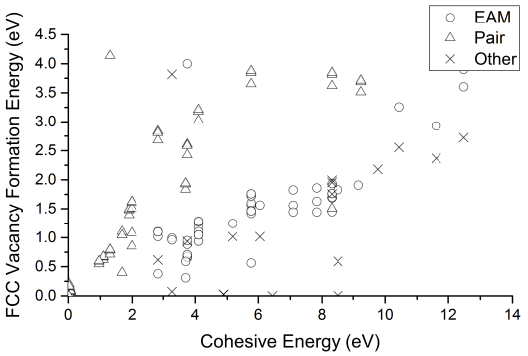

(a)

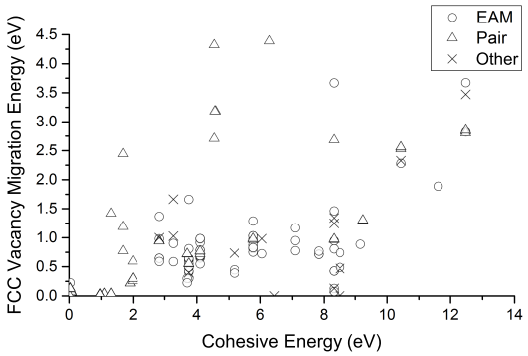

(b)

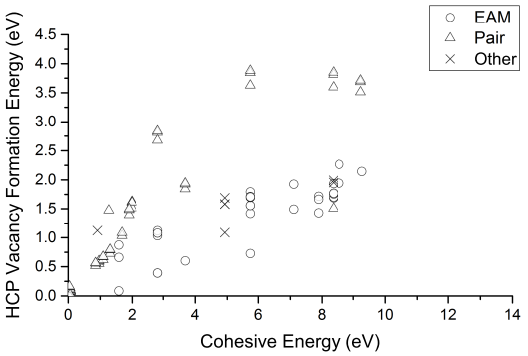

(c)

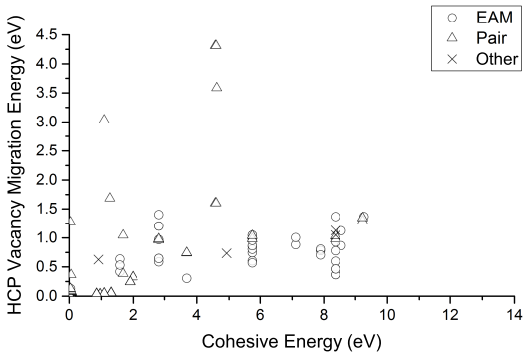

(d)

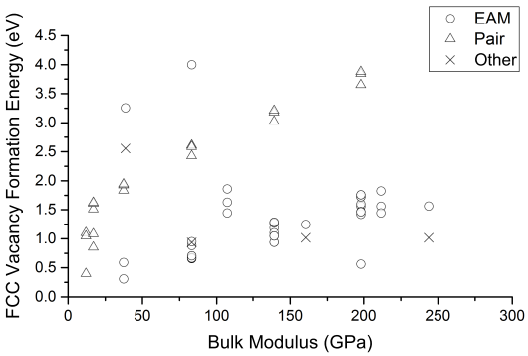

(e)

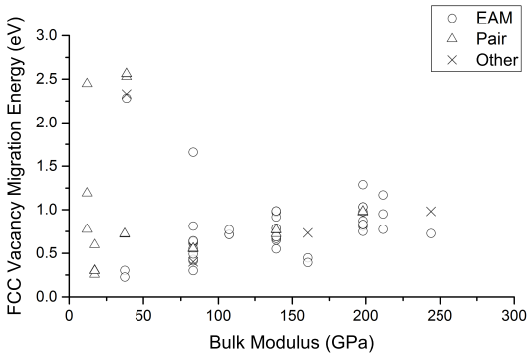

(f)

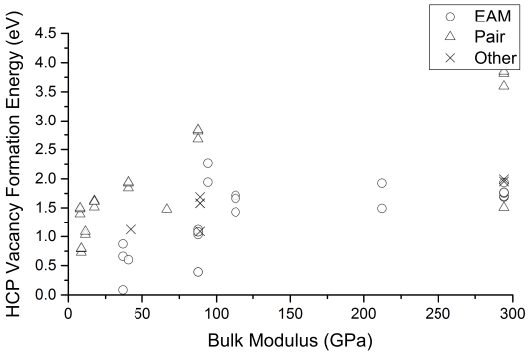

(g)

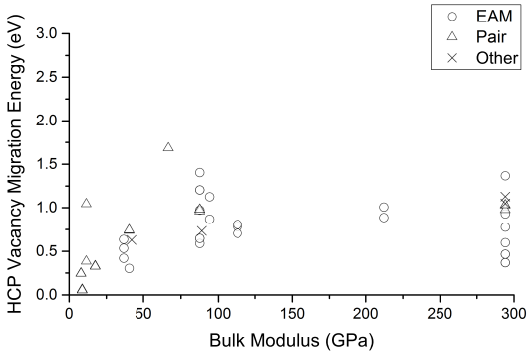

(h)

FIG. 3. VFE and VME versus cohesive energy and bulk modulus.

plotting them on the same graphs. These figures show that the EAM potentials, in general, agree with DFT calculations and experiments, while the pairwise potentials tend to overestimate the vacancy formation energy. We offer an explanation for this: the pairwise potentials neglect the fact that as we remove an atom and create a vacant site, we decrease the number of bonds, which will, in turn, decrease the strength of the remaining bonds and thus the energy change during the relaxation. By using mean absolute percentage error as a measure of the deviation from the reference data to our results, we identify the most promising interatomic models for defect-related simulations for each element. The types of these models agree with our previous analysis: for elements that have EAM potentials, one of the EAM potentials is usually selected as the best model according to the criteria above.

We also plot the results against other elemental properties. The plots show that vacancy formation energy and vacancy migration energy increase with cohesive energy and bulk modulus, which is consistent with previous DFT based studies [16].

V. FUTURE WORKS

First of all, more accurate reference data will be extremely beneficial for improving the accuracy of our assessment. This may be done by improvements in the algorithm used in DFT calculations or the procedure used in experiments. The usage of other computational methods, such as quantum chemistry methods or quantum Monte Carlo may also help.

In addition, the way we select the best models also worth further exploration. The measure used in this study is the mean absolute percentage error, which is widely used but has some biases [17]. It is possible that through some statistical analysis we can get a more suitable measure for this specific situation, and select the best model to perform the calculation we need accordingly, or select multiple models to perform the same calculation and assigning different weight to the result produced by each model accordingly and calculate the weighted average as the final result [18].

Finally, for models with tunable parameters, it would be beneficial to have a unified system that can give the best parameter set (or sets) based on the reference data and the requirement of the user.

Appendix A: Scripts for Retrieving Data From OpenKIM

In this section, we list the scripts for retrieving the data used in this paper from OpenKIM.

Appendix B: Listing of Results

All the results in this work are listed in Table III for archive. The most updated data can be found at the OpenKIM website `https://openkim.org/`.

The calculations are performed with the algorithm described in Section II. The code that implements this algorithm can also be found on the OpenKIM website. Note that for some model-structure pairs, the calculation can't terminate within the time allowed, or produce results that are far from reality. These items are marked as "-" in the two tables mentioned above.

TABLE III: Vacancy formation energy (VFE), migration energy (VME) and relaxation volume (VRV) calculated from atomistic simulations. See Section II for the algorithm used in obtaining these results.

Symbol	Model	VFE (eV)		VME (eV)		VRV ($\AA^3$)	
		fcc	hcp	fcc	hcp	fcc	hcp
Ag	EAM_Dynamo_Ackland_Tichy_Ag	1.02	1.03	0.98	0.97	-	-
Ag	EAM_Dynamo_Hale_Wong_pairHybrid_PdAgH	0.38	0.39	1.37	1.21	-	-
Ag	EAM_Dynamo_Hale_Wong_pairMorse_PdAgH	-	0.39	-	1.21	-	-
Ag	EAM_Dynamo_Williams_Mishin_Ag	1.10	1.08	0.65	0.65	-	-
Ag	EAM_Dynamo_Williams_Mishin_CuAg	1.10	1.08	0.65	0.65	-	-
Ag	EAM_Dynamo_Wu_Trinkle_CuAg	1.10	-	0.65	1.40	-	-
Ag	EAM_Dynamo_Zhou_Johnson_Ag	1.10	1.12	0.59	0.59	-	-
Ag	EMT_Asap_Standard_Jacobsen_Stoltze_Norskov_AlAgAuCuNiPdPt	0.62	-	1.00	-	-	-
Ag	Pair_Morse_Shifted_GirifalcoWeizer_HighCutoff_Ag	2.84	2.84	0.95	0.98	2.20	2.13
Ag	Pair_Morse_Shifted_GirifalcoWeizer_LowCutoff_Ag	2.68	2.68	0.94	0.96	1.98	1.95
Ag	Pair_Morse_Shifted_GirifalcoWeizer_MedCutoff_Ag	2.81	2.81	0.94	0.98	1.79	1.97
Al	EAM_Dynamo_Angelo_Moody_NiAlH	-	0.60	-	0.10	-	-
Al	EAM_Dynamo_Cai_Ye_AlCu	-	-	0.81	0.85	-	-
Al	EAM_Dynamo_Ercolessi_Adams_Al	0.69	0.78	0.61	0.44	-	-
Al	EAM_Dynamo_Mendelev_Asta_AlMg	0.66	0.64	0.64	0.54	-	-
Al	EAM_Dynamo_Mendelev_Kramer_Al	0.66	0.64	0.64	0.54	-	-
Al	EAM_Dynamo_Mendelev_Srolovitz_AlFe	-	0.66	0.41	0.62	-	-
Al	EAM_Dynamo_Mishin_Farkas_Al	0.68	0.74	0.63	0.44	-	-
Al	EAM_Dynamo_Mishin_Mehl_NiAl	4.00	3.31	-	-	-	-
Al	EAM_Dynamo_Mishin_NiAl	0.71	-	0.64	-	-	-

TABLE III: (continued)

Symbol	Model	VFE (eV)		VME (eV)		VRV ($\AA^3$)	
		fcc	hcp	fcc	hcp	fcc	hcp
Al	EAM_Dynamo_PurjaPun_Mishin_NiAl	0.68	-	0.63	1.12	-	-
Al	EAM_Dynamo_Sturgeon_Laird_Al	0.89	-	0.55	-	-	-
Al	EAM_Dynamo_Vailhe_Farkas_CoAl	-	0.68	1.66	0.23	-	-
Al	EAM_Dynamo_Winey_Kubota_Al	0.66	0.64	0.43	0.30	-	-
Al	EAM_Dynamo_Zhou_Johnson_Al	0.67	0.71	0.30	0.26	-	-
Al	EAM_Dynamo_Zope_Mishin_Al	0.71	0.76	0.64	0.49	-	-
Al	EAM_Dynamo_Zope_Mishin_TiAl	0.95	0.76	0.49	0.49	-	-
Al	EMT_Asap_Standard_Jacobsen_Stoltze_Norskov_AlAgAuCuNiPdPt	0.94	-	0.40	-	-	-
Al	Pair_Morse_Shifted_GirifalcoWeizer_HighCutoff_Al	2.61	2.62	0.55	0.60	8.62	3.15
Al	Pair_Morse_Shifted_GirifalcoWeizer_LowCutoff_Al	2.43	2.43	0.55	0.58	3.18	2.57
Al	Pair_Morse_Shifted_GirifalcoWeizer_MedCutoff_Al	2.59	2.59	0.56	0.59	3.35	3.14
Ar	Pair_LJ_Smooth_Bernardes_Ar	0.07	0.07	0.06	0.06	0.77	0.89
Ar	Pair_Lennard_Jones_Shifted_Bernardes_HighCutoff_Ar	0.09	0.09	0.07	0.07	1.36	1.37
Ar	Pair_Morse_Sigmoid_Jelinek_Ar	0.00	0.00	0.00	0.00	-	-
Ar	Pair_Morse_Shifted_Jelinek_Ar	0.09	0.09	0.07	0.07	0.87	0.88
Ar	Pair_Morse_Smoothed90_Jelinek_Ar	0.09	0.09	0.07	0.07	0.86	0.88
Ar	Pair_Lennard_Jones_Shifted_Bernardes_LowCutoff_Ar	0.08	0.08	0.06	0.06	0.93	1.06
Ar	Pair_Lennard_Jones_Truncated_Nguyen_Ar	0.09	0.09	0.08	0.07	-	24.83
Ar	Pair_Lennard_Jones_Shifted_Bernardes_MedCutoff_Ar	0.09	0.09	0.07	0.07	1.34	1.33
Au	EMT_Asap_Standard_Jacobsen_Stoltze_Norskov_AlAgAuCuNiPdPt	0.07	-	1.03	-	-	-
Au	EAM_Dynamo_Zhou_Johnson_Au	1.00	1.02	0.59	0.59	-	-
Au	EAM_Dynamo_Ackland_Tichy_Au	0.96	0.99	0.90	0.90	-	-
Au	MorseEIP_GuthikondaElliott_2011_AuCd	3.82	3.82	1.67	1.70	1.49	1.49
Ca	LennardJones612_Universal	0.85	-	0.26	-	-	-
Ca	Pair_Morse_Shifted_GirifalcoWeizer_LowCutoff_Ca	1.51	1.51	0.30	0.33	9.20	9.21
Ca	LennardJones612_UniversalShifted	1.08	-	0.60	-	-	-
Ca	Pair_Morse_Shifted_GirifalcoWeizer_MedCutoff_Ca	1.61	1.61	0.30	0.33	9.84	9.92
Ca	Pair_Morse_Shifted_GirifalcoWeizer_HighCutoff_Ca	1.63	1.63	0.30	0.33	10.07	10.07
Ba	Pair_Morse_Shifted_GirifalcoWeizer_LowCutoff_Ba	1.40	1.39	0.22	0.25	16.77	16.00
Ba	Pair_Morse_Shifted_GirifalcoWeizer_MedCutoff_Ba	1.48	1.48	0.22	0.25	17.75	17.48
Ba	Pair_Morse_Shifted_GirifalcoWeizer_HighCutoff_Ba	1.50	1.50	0.22	0.25	18.37	17.86
Co	EAM_Dynamo_Zhou_Johnson_Co	1.83	1.93	0.78	0.89	-	-
Co	EAM_Dynamo_PurjaPun_Mishin_Co	1.56	1.49	0.95	1.01	-	-
Co	EAM_Dynamo_Vailhe_Farkas_CoAl	1.44	-	1.17	28.50	-	-
Cr	Pair_Morse_Shifted_GirifalcoWeizer_LowCutoff_Cr	3.51	3.51	1.29	1.29	1.31	2.15
Cr	Pair_Morse_Shifted_GirifalcoWeizer_MedCutoff_Cr	3.69	3.69	1.30	1.35	1.39	1.38
Cr	Pair_Morse_Shifted_GirifalcoWeizer_HighCutoff_Cr	3.72	3.72	1.30	1.35	1.42	1.40
Cu	EAM_Dynamo_Hoyt_Garvin_PbCu	1.28	1.28	0.67	0.67	-	-
Cu	EAM_Dynamo_Cai_Ye_AlCu	1.27	1.27	0.65	0.66	-	-
Cu	EAM_Dynamo_Foiles_Baskes_Universal3_Cu	1.28	1.28	0.67	0.67	-	-
Cu	EAM_Dynamo_Bonny_Pasianot_FeCuNi	1.27	1.25	0.69	0.67	-	-
Cu	EAM_Dynamo_Ackland_Tichy_Cu	1.19	1.20	0.98	0.97	-	-
Cu	EAM_Dynamo_Mendelev_King_Cu	1.11	1.09	0.92	0.89	-	-
Cu	EAM_Dynamo_Onat_Durukanoglu_CuNi	0.94	18.88	0.79	-	-	-
Cu	EAM_Dynamo_Mendelev_Kramer_Cu	1.05	1.04	0.99	0.97	-	-
Cu	EAM_Dynamo_Mishin_Mehl_Cu	1.27	1.25	0.69	0.67	-	-
Cu	EAM_Dynamo_Onat_Durukanoglu_CuNi	0.94	1.24	0.79	0.64	-	-
Cu	EAM_Dynamo_Zhou_Johnson_Cu	1.28	1.32	0.55	0.54	-	-
Cu	Pair_Morse_Shifted_GirifalcoWeizer_LowCutoff_Cu	3.02	3.00	0.72	0.77	1.93	2.60
Cu	EAM_Dynamo_Mendelev_Kramer_CuZr	1.05	1.04	0.99	0.97	-	-
Cu	EAM_Dynamo_Mendelev_Sordelet_CuZr	1.05	1.04	0.99	0.97	-	-
Cu	Pair_Morse_Shifted_GirifalcoWeizer_MedCutoff_Cu	3.18	3.18	0.77	0.81	2.52	2.40
Cu	Pair_Morse_Shifted_GirifalcoWeizer_HighCutoff_Cu	3.21	3.21	0.77	0.82	2.20	2.16
Cd	LennardJones612_Universal	0.30	-	0.31	-	-	-
Cd	MorseEIP_GuthikondaElliott_2011_AuCd	1.12	1.12	0.61	0.63	-	-
Fe	Pair_Johnson_Fe	1.51	1.51	9.74	9.67	0.00	0.00
Fe	model_Fe_PF_DudarevDerlet	1.95	1.95	1.25	1.13	0.61	0.62
Fe	EAM_Dynamo_Ackland_Bacon_Fe	1.94	1.94	1.46	1.37	-	-
Fe	Pair_Morse_Shifted_GirifalcoWeizer_LowCutoff_Fe	3.62	3.60	0.97	0.98	1.83	1.24
Fe	EAM_Dynamo_Zhou_Johnson_Fe	1.69	1.69	0.95	0.78	-	-

TABLE III: (continued)

Symbol	Model	VFE (eV)		VME (eV)		VRV ($\AA^3$)	
		fcc	hcp	fcc	hcp	fcc	hcp
Fe	model_Fe_PF_chiesa_quinticsplines	1.99	1.99	1.34	1.05	1.68	1.68
Fe	model_Fe_PF_mendelev	1.76	-	0.13	-	-	-
Fe	EAM_Dynamo_Mendelev_Han_Fe_2	1.76	1.77	0.13	0.37	-	-
Fe	EAM_Dynamo_Bonny_Pasianot_FeNi	1.45	1.77	3.67	0.37	-	-
Fe	EAM_Dynamo_Mendelev_Han_Fe_5	1.71	1.70	0.81	0.60	-	-
Fe	LennardJones612_Universal	8.42	-	2.69	-	-	-
Fe	EAM_Dynamo_Bonny_Pasianot_FeCuNi	1.70	-	0.08	-	-	-
Fe	EAM_Dynamo_Ackland_Mendelev_FeP	1.76	-	0.43	-	-	-
Fe	EAM_Dynamo_Mendelev_Han_VFe	1.76	1.77	0.43	0.47	-	-
Fe	Pair_Morse_Shifted_GirifalcoWeizer_MedCutoff_Fe	3.81	3.81	0.98	1.03	2.02	1.99
Fe	EAM_Dynamo_Mendelev_Srolovitz_AlFe	1.76	1.76	0.43	0.93	-	-
Fe	Pair_Morse_Shifted_GirifalcoWeizer_HighCutoff_Fe	3.85	3.85	0.98	1.03	2.06	2.06
Fe	EAM_Dynamo_Hepburn_Ackland_FeC	1.76	1.77	0.43	0.47	-	-
He	LennardJones612_UniversalShifted	0.00	0.00	0.00	0.00	-	-
He	LennardJones612_UniversalShifted	0.00	-	0.00	-	-	-
He	LennardJones612_Universal	0.00	0.00	0.00	0.00	-	-
He	LennardJones612_Universal	0.00	0.00	0.00	0.00	-	-
Er	LennardJones612_UniversalShifted	5.88	-	2.71	-	-	-
Er	LennardJones612_Universal	6.20	-	4.32	-	-	-
Kr	Pair_Lennard_Jones_Shifted_Bernardes_LowCutoff_Kr	0.11	0.11	0.08	0.08	1.43	1.42
Kr	LennardJones612_UniversalShifted	-	0.02	-	0.37	-	-
Kr	LennardJones612_UniversalShifted	-	0.14	-	0.08	-	-
Kr	Pair_Lennard_Jones_Shifted_Bernardes_MedCutoff_Kr	0.11	0.11	0.09	0.09	1.60	1.59
Kr	Pair_Lennard_Jones_Shifted_Bernardes_HighCutoff_Kr	0.12	0.12	0.09	0.09	1.64	1.64
Mg	EMT_Asap_MetalGlass_CuMgZr	0.47	-	0.34	-	-	-
Mg	EAM_Dynamo_Zhou_Johnson_Mg	0.68	0.66	0.41	0.42	-	-
Mg	EAM_Dynamo_Sun_Mendelev_Mg	0.86	0.87	0.61	0.64	-	-
Mg	EAM_Dynamo_Mendelev_Asta_AlMg	0.18	0.09	0.78	0.53	-	-
Mg	LennardJones612_Universal	0.66	-	0.49	-	-	-
Cs	Pair_Morse_Shifted_GirifalcoWeizer_LowCutoff_Cs	0.51	0.52	0.03	0.04	47.17	43.60
Cs	Pair_Morse_Shifted_GirifalcoWeizer_MedCutoff_Cs	0.56	0.56	0.03	0.04	-	-
Cs	Pair_Morse_Shifted_GirifalcoWeizer_HighCutoff_Cs	0.57	0.57	0.03	0.04	-	-
Ne	LennardJones612_Universal	0.00	0.00	0.00	0.00	-	-
Ne	Pair_Lennard_Jones_Shifted_Bernardes_LowCutoff_Ne	0.02	0.02	0.02	0.02	0.38	0.38
Ne	Pair_Morse_Shifted_Glyde_Ne	0.03	0.03	0.03	0.03	0.16	0.16
Ne	Pair_Lennard_Jones_Shifted_Bernardes_MedCutoff_Ne	0.03	0.03	0.02	0.02	0.44	0.44
Ne	Pair_Lennard_Jones_Shifted_Bernardes_HighCutoff_Ne	0.03	0.03	0.02	0.02	0.46	0.46
Mo	model_Mo_PF_cubicsplines	2.56	2.56	2.33	2.38	2.47	2.44
Mo	EAM_Dynamo_Zhou_Johnson_Mo	3.25	3.26	2.28	2.13	-	-
Mo	Pair_Morse_Shifted_GirifalcoWeizer_LowCutoff_Mo	6.20	6.22	2.53	2.61	1.50	1.45
Mo	EAM_Dynamo_Smirnova_UMoXe	-	-	-	0.80	-	-
Mo	Pair_Morse_Shifted_GirifalcoWeizer_MedCutoff_Mo	6.50	6.51	2.56	2.63	1.57	1.56
Mo	Pair_Morse_Shifted_GirifalcoWeizer_HighCutoff_Mo	6.56	6.56	2.56	2.63	1.60	2.27
Nb	model_Nb_PF_cubicsplines	2.18	-	-	-	-	8.40
Ni	EAM_Dynamo_Ackland_Tichy_Ni	1.42	1.42	0.81	0.86	-	-
Ni	EAM_Dynamo_Bonny_Pasianot_FeNi	1.56	1.79	0.98	0.61	-	-
Ni	EAM_Dynamo_Mishin_Mehl_NiAl	0.56	0.73	1.03	0.87	-	-
Ni	EAM_Dynamo_Bonny_Pasianot_FeCuNi	1.72	1.71	0.75	0.75	-	-
Ni	EAM_Dynamo_Mishin_Farkas_Ni	1.60	-	1.29	-	-	-
Ni	EAM_Dynamo_Zhou_Johnson_Ni	1.72	1.70	0.87	0.80	-	-
Ni	EAM_Dynamo_Onat_Durukanoglu_CuNi	1.47	1.70	0.83	0.57	-	-
Ni	Pair_Morse_Shifted_GirifalcoWeizer_LowCutoff_Ni	3.65	3.63	0.97	0.98	1.71	1.16
Ni	EAM_Dynamo_Mendelev_Ni	1.76	1.71	1.03	0.96	-	-
Ni	EAM_Dynamo_Onat_Durukanoglu_CuNi	1.46	49.58	0.83	-	-	-
Ni	EAM_Dynamo_Mishin_NiAl	-	1.56	-	1.05	-	-
Ni	EAM_Dynamo_PurjaPun_Mishin_NiAl	-	1.56	-	1.05	-	-
Ni	Pair_Morse_Shifted_GirifalcoWeizer_MedCutoff_Ni	3.84	3.84	0.98	1.04	1.90	1.89
Ni	EAM_Dynamo_Mendelev_NiZr	1.76	-	1.03	-	-	-
Ni	Pair_Morse_Shifted_GirifalcoWeizer_HighCutoff_Ni	3.88	3.88	0.98	1.04	1.93	1.72
Na	LennardJones612_UniversalShifted	4.14	-	1.42	-	-	-

TABLE III: (continued)

Symbol	Model	VFE (eV)		VME (eV)		VRV ($\AA^3$)	
		fcc	hcp	fcc	hcp	fcc	hcp
Na	Pair_Morse_Shifted_GirifalcoWeizer_LowCutoff_Na	0.72	0.73	0.04	0.06	12.33	15.17
Na	Pair_Morse_Shifted_GirifalcoWeizer_MedCutoff_Na	0.79	0.79	0.04	0.06	18.10	16.49
Na	Pair_Morse_Shifted_GirifalcoWeizer_HighCutoff_Na	0.80	0.80	0.04	0.06	18.78	19.56
Pb	EAM_Dynamo_Zhou_Johnson_Pb	0.59	0.60	0.30	0.31	-	-
Pb	EAM_Dynamo_Landa_Wynblatt_AlPb	0.31	-	0.23	-	-	-
Pb	Pair_Morse_Shifted_GirifalcoWeizer_LowCutoff_Pb	1.84	1.84	0.72	0.74	3.06	2.99
Pb	Pair_Morse_Shifted_GirifalcoWeizer_MedCutoff_Pb	1.93	1.93	0.72	0.75	3.22	3.26
Pb	Pair_Morse_Shifted_GirifalcoWeizer_HighCutoff_Pb	1.94	1.94	0.73	0.75	3.17	3.27
Pd	EMT_Asap_Standard_Jacobsen_Stoltze_Norskov_AlAgAuCuNiPdPt	1.02	-	0.73	-	-	-
Pd	EAM_Dynamo_Hale_Wong_pairHybrid_PdAgH	1.25	1.35	0.45	0.33	-	-
Pd	EAM_Dynamo_Hale_Wong_pairMorse_PdAgH	-	1.35	0.39	0.33	-	-
Dy	LennardJones612_UniversalShifted	5.65	-	3.18	-	-	-
Dy	LennardJones612_Universal	5.68	-	4.99	1.60	-	-
Pt	EAM_Dynamo_Zhou_Johnson_Pt	1.56	1.66	0.73	0.65	-	-
Pt	EMT_Asap_Standard_Jacobsen_Stoltze_Norskov_AlAgAuCuNiPdPt	1.02	-	0.98	-	-	-
K	Pair_Morse_Shifted_GirifalcoWeizer_LowCutoff_K	0.62	0.62	0.04	0.05	-	33.47
K	Pair_Morse_Shifted_GirifalcoWeizer_MedCutoff_K	0.66	0.67	0.04	0.05	31.68	35.84
K	Pair_Morse_Shifted_GirifalcoWeizer_HighCutoff_K	0.67	0.68	0.04	0.05	32.09	33.01
Ru	EAM_Dynamo_Fortini_Mendelev_Ru	1.91	2.15	0.89	1.37	-	-
Ho	LennardJones612_Universal	5.68	-	4.99	1.60	-	-
Ho	LennardJones612_UniversalShifted	5.65	-	3.18	-	-	-
Ta	EAM_Dynamo_Li_Siegel_Ta	2.93	2.93	1.89	1.74	-	-
Ta	model_Ta_PF_cubicsplines_derletnguyenmanhdudarev	2.37	2.48	-	-	-	7.61
Ti	EAM_Dynamo_Ackland_Ti	1.45	1.43	0.72	0.78	-	-
Ti	EAM_Dynamo_Zhou_Johnson_Ti	1.63	1.72	0.71	0.81	-	-
Ti	EAM_Dynamo_Zope_Mishin_TiAl	1.86	1.66	0.77	0.71	-	-
Si	Three_Body_Stillinger_Weber_Balamane_Si	0.03	1.69	-	-	-	0.96
Si	Three_Body_Stillinger_Weber_Si	0.02	1.58	-	-	-	0.99
Si	Three_Body_Stillinger_Weber_Si	0.02	1.58	-	-	-	0.99
Si	Three_Body_Stillinger_Weber_Zhang_Silicene_Model1_Si	-	1.09	-	0.73	-	4.22
W	EAM_Dynamo_Zhou_Johnson_W	3.91	3.91	2.82	2.65	-	-
W	model_W_PF_cubicsplines	2.72	2.72	3.47	3.37	1.81	1.81
W	EAM_Dynamo_Ackland_W	3.60	3.60	3.67	3.11	-	-
W	Pair_Morse_Shifted_GirifalcoWeizer_LowCutoff_W	7.97	7.96	2.83	2.88	1.80	1.79
W	Pair_Morse_Shifted_GirifalcoWeizer_MedCutoff_W	8.36	8.36	2.80	2.92	2.56	2.05
W	Pair_Morse_Shifted_GirifalcoWeizer_HighCutoff_W	8.43	8.43	2.85	2.94	1.97	1.94
Y	Dipole_Umeno_YSZ	0.00	-	0.00	-	-	-
Xe	Pair_Lennard_Jones_Shifted_Bernardes_LowCutoff_Xe	0.15	0.15	0.12	0.12	1.95	1.95
Xe	EAM_Dynamo_Smirnova_UMoXe	-	0.00	0.23	0.13	-	-
Xe	LennardJones612_Universal	0.20	-	0.14	-	-	-
Xe	Pair_Lennard_Jones_Shifted_Bernardes_MedCutoff_Xe	0.16	0.16	0.12	0.13	2.04	2.03
Xe	Pair_Lennard_Jones_Shifted_Bernardes_HighCutoff_Xe	0.17	0.17	0.13	0.13	2.09	2.09
Zr	Dipole_Umeno_YSZ	0.00	-	0.00	-	-	-
Zr	EMT_Asap_MetalGlass_CuMgZr	0.59	-	0.47	-	-	-
Zr	EAM_Dynamo_Zhou_Johnson_Zr	1.83	1.94	0.74	0.87	-	-
Zr	EAM_Dynamo_Mendelev_Kramer_CuZr	-	-	0.49	-	-	-
Sr	LennardJones612_UniversalShifted	1.10	-	0.77	-	-	-
Sr	LennardJones612_Universal	1.05	1.03	1.19	0.39	-	-
Sr	LennardJones612_UniversalShifted	0.40	-	2.45	-	-	-
Sc	LennardJones612_UniversalShifted	12.17	-	4.39	-	-	-
Rb	Pair_Morse_Shifted_GirifalcoWeizer_LowCutoff_Rb	0.55	0.55	0.03	0.04	39.08	41.53
Rb	Pair_Morse_Shifted_GirifalcoWeizer_MedCutoff_Rb	0.59	0.59	0.02	0.04	43.31	44.28
Rb	Pair_Morse_Shifted_GirifalcoWeizer_HighCutoff_Rb	0.60	0.60	0.02	0.03	45.54	45.31
V	model_V_PF_cubicsplines_derletnguyenmanhdudarev	-	-	-	-	-	3.51
Al	EAM_Dynamo_Landa_Wynblatt_AlPb	-	0.76	-	0.42	-	-
Ar	LennardJones612_UniversalShifted	-	0.10	-	0.08	-	-
Cu	EAM_Dynamo_Wu_Trinkle_CuAg	-	0.83	-	0.42	-	-
Ne	LennardJones612_Universal	-	0.00	-	0.00	-	-
K	LennardJones612_Universal	-	4.62	-	3.03	-	-
Dy	LennardJones612_Universal	-	5.77	-	4.31	-	-

TABLE III: (continued)

Symbol	Model	VFE (eV)		VME (eV)		VRV ($\mathring{A}^3$)	
		fcc	hcp	fcc	hcp	fcc	hcp
Xe	LennardJones612_UniversalShifted	-	-	-	1.28	-	-
Sr	LennardJones612_Universal	-	1.09	-	1.04	-	-
Ho	LennardJones612_Universal	-	5.77	-	4.31	-	-
Zr	EAM_Dynamo_Mendelev_NiZr	-	2.27	-	1.13	-	-
Er	LennardJones612_Universal	-	6.31	-	4.94	-	-
Tb	LennardJones612_Universal	-	10.33	-	3.59	-	-
Pa	LennardJones612_Universal	-	9.60	-	4.76	-	-
Y	LennardJones612_Universal	-	16.86	-	5.40	-	-
Zn	LennardJones612_UniversalShifted	-	1.48	-	1.69	-	-

TABLE IV: In this table, we list the models currently available on OpenKIM that are most consistent with DFT and experiments. They are selected based on the mean absolute percentage error (MAPE) between the vacancy property results they produce and the reference data we have. Here n is the number of vacancy-related reference data available for these models.

Symbol	Model	n	MAPE
Ag	EAM_Dynamo_Zhou_Johnson_Ag	6	24.11%
Al	EAM_Dynamo_Mishin_Farkas_Al	6	8.00%
Au	EAM_Dynamo_Zhou_Johnson_Au	6	60.40%
Ba	Pair_Morse_Shifted_GirifalcoWeizer_LowCutoff_Ba	4	30.48%
Ca	Pair_Morse_Shifted_GirifalcoWeizer_LowCutoff_Ca	6	33.00%
Cd	LennardJones612_Universal	2	18.47%
Co	EAM_Dynamo_PurjaPun_Mishin_Co	4	17.22%
Cs	Pair_Morse_Shifted_GirifalcoWeizer_LowCutoff_Cs	4	64.49%
Cu	EAM_Dynamo_Onat_Durukanoglu_CuNi	6	9.02%
Fe	EAM_Dynamo_Ackland_Bacon_Fe	6	17.21%
K	Pair_Morse_Shifted_GirifalcoWeizer_LowCutoff_K	4	73.45%
Kr	Pair_Lennard_Jones_Shifted_Bernardes_LowCutoff_Kr	2	20.38%
Mg	EAM_Dynamo_Zhou_Johnson_Mg	6	8.60%
Na	Pair_Morse_Shifted_GirifalcoWeizer_LowCutoff_Na	2	79.50%
Ni	EAM_Dynamo_Ackland_Tichy_Ni	4	9.30%
Pb	EAM_Dynamo_Zhou_Johnson_Pb	6	36.27%
Pd	EMT_Asap_Standard_Jacobsen_Stoltze_Norskov_AlAgAuCuNiPdPt	4	21.45%
Pt	EAM_Dynamo_Zhou_Johnson_Pt	6	64.98%
Rb	Pair_Morse_Shifted_GirifalcoWeizer_LowCutoff_Rb	4	75.66%
Ru	EAM_Dynamo_Fortini_Mendelev_Ru	4	33.26%
Sr	LennardJones612_UniversalShifted	2	43.93%
Ta	model_Ta_PF_cubicsplines_derletnguyenmanhdudarev	2	5.88%
Ti	EAM_Dynamo_Zope_Mishin_TiAl	6	33.57%
W	model_W_PF_cubicsplines	2	37.38%
Zr	EAM_Dynamo_Zhou_Johnson_Zr	5	21.83%
Mo	model_Mo_PF_cubicsplines	1	30.54%

[1] M. S. Daw, S. M. Foiles, and M. I. Baskes, Materials Science Reports **9**, 251 (1993).

[2] M. S. Daw and M. I. Baskes, Physical Review B **29**, 6443 (1984).

[3] M. Bierbaum, E. Tadmor, R. Elliott, T. Wennblom, A. Alemi, Y.-J. Chen, D. Karls, A. Ludvik, and J. Sethna, in *APS Meeting Abstracts*, Vol. 1 (2014) p. 26004.

[4] "OpenKIM: Knowledgebase of Interatomic Models," `https://openkim.org/`, [Online; accessed 11-February-2016].

[5] E. Tadmor, R. Elliott, J. Sethna, R. Miller, and C. Becker, JOM Journal of the Minerals, Metals and Materials Society **63**, 17 (2011).

[6] J. Weertman, Journal of Applied Physics **26**, 1213 (1955).

[7] P. M. Fahey, P. Griffin, and J. Plummer, Reviews of modern physics **61**, 289 (1989).

[8] J. Sethna, "Crystals, Rigidity, and Statistical Mechanics," `http://pages.physics.cornell.edu/~sethna/teaching/BasicTraining/BasicTraining.html` (2014), [Online; accessed 09-February-2016].

[9] B. Andreas, Y. Azuma, G. Bartl, P. Becker, H. Bettin,

M. Borys, I. Busch, P. Fuchs, K. Fujii, H. Fujimoto, *et al.*, Metrologia **48**, S1 (2011).
[10] S. R. Bahn and K. W. Jacobsen, Computing in Science & Engineering **4**, 56 (2002).
[11] L. D. Landau and E. M. Lifshitz, *Course of theoretical physics* (Elsevier, 2013).
[12] C. Freysoldt, B. Grabowski, T. Hickel, J. Neugebauer, G. Kresse, A. Janotti, and C. G. Van de Walle, Reviews of Modern Physics **86**, 253 (2014).
[13] Y. Mishin, D. Farkas, M. Mehl, and D. Papaconstantopoulos, Physical Review B **59**, 3393 (1999).
[14] A. Jain, S. P. Ong, G. Hautier, W. Chen, W. D. Richards, S. Dacek, S. Cholia, D. Gunter, D. Skinner, G. Ceder, *et al.*, Apl Materials **1**, 011002 (2013).
[15] M. De Jong, W. Chen, T. Angsten, A. Jain, R. Notestine, A. Gamst, M. Sluiter, C. K. Ande, S. van der Zwaag, J. J. Plata, *et al.*, Scientific data **2** (2015).
[16] T. Angsten, T. Mayeshiba, H. Wu, and D. Morgan, New Journal of Physics **16**, 015018 (2014).
[17] D. Mayer and D. Butler, Ecological modelling **68**, 21 (1993).
[18] S. L. Frederiksen, K. W. Jacobsen, K. S. Brown, and J. P. Sethna, Physical review letters **93**, 165501 (2004).
[19] M. Baskes, M. Daw, and S. Foiles, in *MRS Proceedings*, Vol. 141 (Cambridge Univ Press, 1988) p. 31.
[20] A. Carlsson, Solid State Physics **43**, 1 (1990).
[21] B. Medasani, M. Haranczyk, A. Canning, and M. Asta, Computational Materials Science **101**, 96 (2015).
[22] E. Bitzek, P. Koskinen, F. Gähler, M. Moseler, and P. Gumbsch, Physical review letters **97**, 170201 (2006).
[23] T. E. Oliphant, Computing in Science & Engineering **9**, 10 (2007).
[24] J. A. Nelder and R. Mead, The computer journal **7**, 308 (1965).
[25] S. G. Louie, M. Schlüter, J. R. Chelikowsky, and M. L. Cohen, Physical Review B **13**, 1654 (1976).
[26] A. F. Voter, F. Montalenti, and T. C. Germann, Annual Review of Materials Research **32**, 321 (2002).
[27] T. Suzuki, I. Kosacki, and H. U. Anderson, Solid State Ionics **151**, 111 (2002).
[28] A. Kalabukhov, R. Gunnarsson, J. Börjesson, E. Olsson, T. Claeson, and D. Winkler, Physical Review B **75**, 121404 (2007).
[29] J.-E. Kluin and T. Hehenkamp, Physical Review B **44**, 11597 (1991).
[30] M. Kass, C. R. Brooks, D. Falcon, and D. Basak, Intermetallics **10**, 951 (2002).
[31] Y. Kraftmakher, Physics Reports **299**, 79 (1998).
[32] P. Shewmon, The Minerals, Metals & Materials Society, Diffusion in Solids. Second Edition.(Retroactive Coverage)(United States), 1989, , 246 (1989).
[33] J. K. Nørskov, T. Bligaard, J. Rossmeisl, and C. H. Christensen, Nature chemistry **1**, 37 (2009).
[34] R. Bourassa and B. Lengeler, Journal of Physics F: Metal Physics **6**, 1405 (1976).
[35] B. McKee, W. Triftshäuser, and A. Stewart, Physical Review Letters **28**, 358 (1972).
[36] T. Korhonen, M. Puska, and R. Nieminen, Physical Review B **51**, 9526 (1995).
[37] W. Kohn, Reviews of Modern Physics **71**, 1253 (1999).
[38] W. Foulkes, L. Mitas, R. Needs, and G. Rajagopal, Reviews of Modern Physics **73**, 33 (2001).
[39] J. Kotakoski, A. Krasheninnikov, and K. Nordlund, Physical Review B **74**, 245420 (2006).
[40] H. Zhou, S. Upreti, N. A. Chernova, G. Hautier, G. Ceder, and M. S. Whittingham, Chemistry of Materials **23**, 293 (2010).
[41] G. Ceder, MRS bulletin **35**, 693 (2010).